Layer Adhesion Control in 3D Printed Silicone Using Curing Kinetics

Stephanie Walker[a*], Emma Lingle[a], T.J. Wallin[b], Kate Healy[b], Yiğit Mengüç[b], Joseph Davidson[a]

a. CoRIS Institute, Oregon State University, 204 Rogers Hall, Corvallis, OR 97331, USA, *walkers@oregonstate.edu (corresponding author), joseph.davidson@oregonstate.edu

b. Facebook Reality Labs, Redmond, WA, USA.

Highlights (will go in a separate word document – here for review only, 85 char per line, general audience)

- Adhesive forces between curing thermoset layers decrease as cure % increases
- Less permanent bonding sites at higher cure % decrease ultimate interfacial strength
- Ecoflex 00-30 peel strength decreases after ~ 1% cure
- Tracking adhesion for path planning must occur in the future to ensure predictable mechanical properties

ABSTRACT

Adhesion in layer-by-layer fabrication is dictated by many physical and chemical interactions at the manufactured interface. To properly adhere two materials together, interfaces are often manipulated or optimized to ensure the desired bond strength between two or more substrates. Direct ink writing materials, in this case thermoset polymers, depend on these bond strengths for predictable mechanical performance in the finished part. However, the role of cure in the development of interfacial adhesive forces for thermoset silicone has yet to be demonstrated for direct ink writing. Here, we report the cure testing, fabrication, and characterization of curing thermoset silicone samples of differing cure percent in the context of ultimate adhesive force. Using differential scanning calorimetry (DSC) and peel testing, we report the expected cure rate and cure percent behavior over time and examine the range of adhesive forces possible when layering a curing silicone thermoset. Adhesive data will improve nozzle path planning in direct ink writing to help achieve higher peel forces and more predictable mechanical properties.

Introduction

Direct ink writing is a promising method of 3D printing soft liquid polymers and other fluids. These liquid precursors are extruded into 3D shapes that then undergo subsequent chemical crosslinking reactions, or other post-processing, to produce a finished three-dimensional part. Thermoset elastomers, particularly silicone, are good candidates for direct ink writing because they usually come packaged as separate liquids of low viscosity that cure after mixing (CITE). Use of thermosetting elastomers for direct ink writing is an active field of research in several applications, including the creation of multi-material voxelated parts[1], control of printed resolution using fluid deformation/instability/fracture[2], exploration of mixing techniques[3], printing of soft materials into high resolution parts within a supportive bath[4–6], extrusion of multi-layered concentric sensors[7], silicone extrusion patterning[8],printing with silicone microbeads[9], printing silicone onto a conformable 3D surface[10,11], tuning 3D printable silicone

material properties[12], multimaterial printing with silicone and wax[13], and developing zero-support methods of printing soft silicone[14].

Generally, direct ink writing materials are difficult to 3D print without some rheological modification(s) or support bath structures due to their inherent softness and low viscosity. Material design must ensure uninterrupted flow through the printing nozzle and substantive strength after extrusion for 3D layering and overhanging geometries. Rheological modifications generally increase the yield stress, control the viscoelastic parameters like elastic modulus (G′), control viscosity, and promote shear thinning[15] in the inks. A high yield stress prevents slumping and collapse of the extruded material during printing. The material is ideally G′ dominated for solid-like (versus liquid-like) behavior in the fluid, but G′ should not be so high as to prevent extrusion entirely. Viscosity is essentially resistance to flow, so lowering viscosity enough to flow through the nozzle may be necessary. Shear thinning properties in the fluid align the polymer chains in high shear regions like the nozzle to lower the viscosity for lower pressure extrusion.

Direct ink writing of thermosetting elastomers requires another important modification to either the printed fluid or the printing process – control of the curing kinetics. Polymers are either slow-curing or pre-mixed with a cure retarder to prevent material clogging the nozzle or mixed just before extrusion to quickly push the curing material out of the nozzle before it begins to solidify. Direct ink writing of curing thermoset elastomers is a non-trivial process if curing speed is not slowed down. A changing cure rate during printing coordinates with changing rheological properties, such as growth of G′ [14] and increase in viscosity, which can clog the nozzle. Increasing the temperature of the curing thermoset will also increase the cure rate, so the temperature environment should be strictly controlled to reduce variability in the rheological and curing behavior.

Managing curing kinetics, rheology, and temperature are necessary for a dependable thermoset direct ink writing process. We previously developed a framework for characterizing these parameters for arbitrary thermoset materials, developed formulation strategies, rheological control, curing kinetics characterization, and geometrical design rules for their implementation in a custom-built active mixing 3D printer, and applied these rules to print several example parts with significant overhanging geometries (up to 45 degrees). Our previous work used a custom-made open-source high resolution silicone 3D printer to directly print complex elastomeric structures without support[14]. This printer incorporated an in-line mixer to actively mix two parts of a custom RTV-2 silicone just before extrusion and is enclosed in a heated chamber. These modifications permit a greater degree of control over the silicone's curing process without the need to chemically alter the cure speed of the silicone. The elevated temperatures ensure that previously printed layers rapidly cure and therefore develop more strength as the print progresses until they reach a solid state. This structure development allowed spanning features, inaccessible in conventional systems, to hold their shape during printing. To prevent curing in the mixer and nozzle while also increasing the cure speed of layers as much as possible, the system was characterized for curing kinetics and rheology to define an optimal printing time window and maximum operating temperature. Zero-support overhanging structures could be made with liquid silicone rubber (LSR), but this investigation failed to assess the potential impacts to final device performance. It is simple to intuit that as a layer cures over time, there are fewer crosslinkable

groups available for bonding to the subsequent layer. Inadequate crosslinking between layers can lead to anisotropy and premature failure, i.e, delamination at stresses below the ultimate strength of the base material. As the build time for each layer is dependent on the cross-sectional area, individual layers may experience drastically different layer deposition times, and therefore, extent of curing reaction, before the deposition of the next silicone layer. 3D parts with complex geometry will require custom path planning strategies to include the cure percent in the polymer deposition pattern. Determining adhesive force at each interface at different cure times is integral to prediction of mechanical performance and therefore predictability of the 3D printing process.

In this work, we expand upon our existing framework for direct ink writing of a thermoset silicone. We have developed a new formulation for printing based on Ecoflex 00-30, characterized its rheology, and determined its printing suitability (characterization not included in this paper). We use this suitable thermoset silicone to explore how curing kinetics affect adhesion strength in direct ink writing. Isothermal differential scanning calorimetry (DSC) was performed for three possible printing temperatures to determine a range of timings for the silicone curing kinetics. The maximum printing temperature (60°C) in this system was determined within these ranges by running multiple prints in the printer system at temperature without clogging. To remove the quality of mixing as a parameter, we machine mixed the silicone and spread the layers by hand inside the pre-heated printer chamber. Samples were prepared using timed film spreading of 2 layers to control the cure percent of the bottom layer before the addition of the top layer. Adhesion forces were determined in these samples using a T-Peel test method. With a line of best fit, these data model the expected adhesion strength of silicone printed parts in this system. The data show that a low cure percent before new layer deposition (more interfacial bonds available) leads to higher strength parts, and higher cure percent before new layer deposition (less interfacial bonds available) leads to lower strength parts. To create a dependable direct ink writing process, this adhesion data must be eventually integrated into path planning algorithms to control the ultimate strength of printed parts.

Background

Platinum cure silicone chemistry is typically an addition reaction (hydrosilylation) between two prepared and mixed parts with no byproducts[16]. This type of reaction produces a crosslinked thermoset silicone connected via covalent bonds. In silicones like the RTV-2 Ecoflex 00-30, as temperature increases, the rate of crosslinking also increases, enabling thermal control of the curing kinetics. Before the silicone is fully cured and (theoretically) all precursors have been crosslinked into a polymer structure, there are unreacted precursors still in the mixture, which diffuse through the network to react with one another[17]. If the silicone is isothermal and above a few microns in thickness[18], all of the material should have the same curing kinetics. The cure percent (α) of the mixed and printed silicone is determined using differential scanning calorimetry (DSC). Isothermal DSC data (Watts/gram of sample versus time) is used to calculate the rate of cure using the instantaneous heat flow divided by the total heat integral under the heat flow curve. A running integral of the heat flow data divided by the total heat integral gives the cure percent. Because each bonding process releases a specific amount of energy, it is assumed that the heat flow is directly proportional to cure percent.

The types of adhesion possible between layers during the curing phase of an addition cure silicone depend on the specific chemistry, but generally include covalent bonding between the reactive sites (in this case, even though the Ecoflex formulation is proprietary, we expect vinyl ($-CH=CH_2$) and silicon hydride (Si-H) groups) based on platinum-curing silicone chemistry, and intermolecular (van der Waals) bonds between all parts of the mixture (dipole-dipole, London dispersion, induced dipole, and hydrogen bonds). Additives included in the formulation (ex: silica) also can affect adhesive material properties based on their aggregation, pore volume, and polymer-filler attachments[19,20]. Polymer chain entanglements also can serve as effective crosslinks, adding to overall adhesion[21]. Adhesion is also dependent on processing conditions such as the interfacial surface area available for contact, which changes in the presence of imperfect deposition such as air pockets or irregular surfaces.

Quantifying the exact types of adhesive forces in the curing layers is beyond the scope of this text, but we can assume that the more crosslinking that occurs at an interface, the more that the interface will resist peeling apart due to the formation of more covalent bonds. Cure percent, a quantification of the number of crosslinks in a curing material, can be correlated to adhesive peel strength in thermoset layers. A T-Peel test characterizes this correlation by quantifying the peel resistance via adhesion forces (force/width of sample) between the two layers[22]. The data from the T-Peel test generally show a peak of initiation force followed by a range of crack propagation forces that peel the sample until break. Peel sample geometry, plastic or elastic deformation in the peel arms/tabs, energy dissipation effects, material composition, temperature, separation rate, interface effects, test angle, and equipment can affect peel test results[23–26]. The initiation of the peel also has its own complexities depending on the sharpness of the crack and the types of stress distributions at the crack front[24]. The ideal failure mode in a layered part is 100% cohesive failure, in which the adhesive bond is strong enough to cause the bulk material to break before peeling only at the interface. Adhesive failure (occurring only at the interface) means that the weakest area of the printed part is between printed layers. A mixture of cohesive and adhesive failure can also occur[27] (Figure 2).

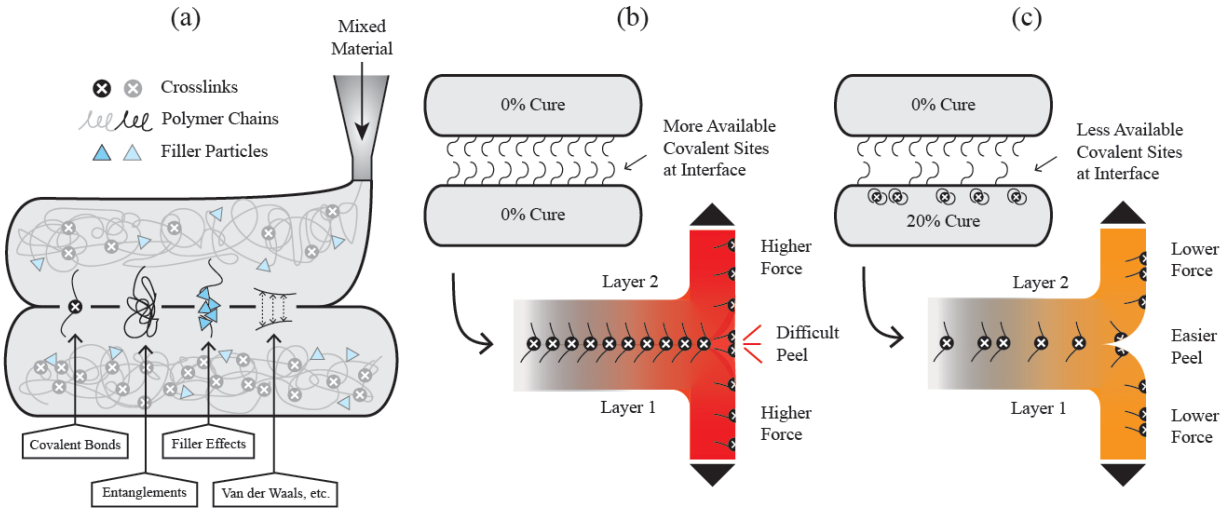

Figure 1. (a) Conceptual drawing of some adhesion contributors between curing layers during 3D extrusion and layering. (b) General crosslinking and peeling behavior between two uncured layers. (c) General crosslinking and peeling behavior of two layers, with one layer being partially cured.

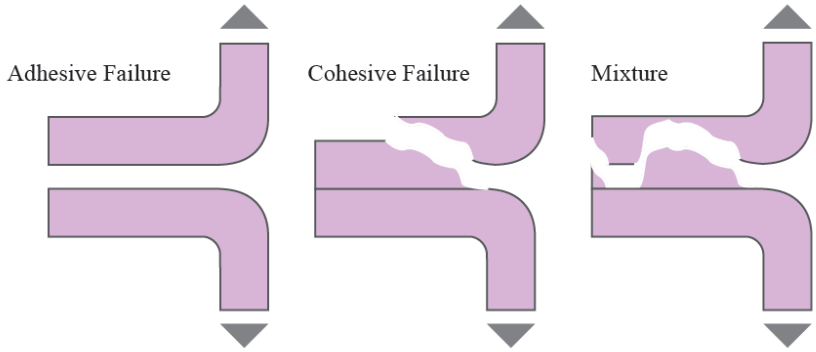

Figure 2. In peel testing, adhesive, cohesive, and a mixture of both cohesive and adhesive failure can occur. For 3D printed part strength, 100% cohesive failure is the goal. Cohesive failure occurs when the adhered interface is as strong or stronger than the bulk material bonds. Adhesive failure occurs when the interface is weaker than the bulk material bonds.

While previous work in direct ink writing of thermosets focused on rheological modifiers and altering reaction rates for rapid shape fixity, the impact on interlayer adhesion remains unclear. Past work has assumed proper layer adhesion as long as the layers were deposited before the silicone fully cured[28], relied on full curing of the previous layer before a new layer was deposited to ensure adequate structural integrity[29], or did not focus on layer adhesion in the work[14]. Layer-to-layer adhesion research in thermosets is more common in stereolithography printing, where ultraviolet (UV) or infrared (IR) light is passed through a layer of uncured resin or a focused voxel within a bath to build 3D structures[30]. Silicone has been 3D printed with these methods[31,32]. The bonding between layers is permanent, and light bleed-through from the curing layer to the previously irradiated layer creates a layer-to-layer bond[33,34]. The amount of cure depends on the light intensity, exposure time, as well as the specific polymer chemistry[35]. In UV-cured chemistry as well as thermoset chemistry presented here, control of the curing kinetics is integral to proper printed part strength and dimensional accuracy.

Silicone adhesion between layers also has implications for soft device fabrication outside of 3D printing. Soft lithography is a common method to adhere two silicone parts together. Often, a newly-mixed and uncured silicone is used as an adhesive for 2 or more silicone parts[36–38]. While the maximum strength of adhesion is not usually tested, it is assumed that the adhesion between the cured and uncured silicone is sufficient for the intended task. This type of adhesion is especially important in inflatable structures which often fail at these glued seams. Knowing the point of failure before building a soft device is an important step to improving its manufacturing process.

Experimental Methodologies

Silicone preparation

Ecoflex 00-30 (EF) (Smooth-On) was used as the base polymer. Thi-Vex and Urefil-9 were added, resulting in the following mixtures: (Part A) 44.5 g EF Part A, 0.5 g TV, 1.0 g Urefil-9 and (Part B) 44.5 g EF Part A, 0.5 g TV, 1.0 g Urefil-9. Each component (Part A Mixture and B Mixture) was each mixed in a Thinky ARE-310 Planetary mixer for 30 s at 2000 rpm and 30 seconds at 2200 rpm. The mixed parts were then loaded into their separate syringes using a spatula. Part A and Part B were used for DSC tests as-is. To remove bubbles for film spre from this highly viscous yield stress fluid, a few additional steps were taken. First, each full syringe was divided into two syringes by extruding half the volume of one syringe into a new syringe. Second, the syringe plungers were compressed to push all the material towards the syringe tip, and then quickly removed to spread the material over the inner walls of the syringe. We found it easier to vacuum out the bubbles from the thin layer of material on the walls of the syringe rather than in a large volume in a cup. The syringes were vacuumed without plungers at approximately -100 kPa for 30 minutes, and then the plungers were replaced and two syringes (of the same Part A or B) were recombined into one syringe for experiments.

Curing Kinetics Testing

Curing kinetics of the thermoset silicones were determined on a DSC Q2000 (TA instruments) using isothermal temperature scans. Approximately 2 g Part A and 2 g Part B were mixed in a Thinky ARE-310 Planetary mixer for 2000 rpm for 30 s and then 2200 rpm for 30 s at room temperature. The sample was then quickly loaded into a syringe with an attached nozzle and syringed into the hermetic pan, noting the mass of the sample. Sample masses ranged from 13.8 mg to 18.7 mg. The lid was then quickly clamped onto the pan and the sample was loaded into the DSC. Samples were loaded into the pre-heated DSC by approximately 2 minutes from mixing. The sample (silicone + aluminum hermetic pan and lid) and reference (aluminum hermetic pan and lid only) were placed in the isothermal furnace for approximately 30 minutes and heat flow coming from the sample pan was recorded over time. Five samples were run per temperature. The heat flow curves represent the heat given off by the sample during curing, with exothermic data in the positive direction. It was assumed that every bond made in the curing silicone released the same amount of exothermic heat, and so the heat flow of the sample was proportional to the cure rate. The isothermal silicone samples generally had a heat flow curve that grew into a peak and then decreased until reaching a region of no heat flow change. The beginning of the region with no heat flow change at the end of the run was the cure point (with the assumption of no additional reactions). Because of the assumption of proportionality described earlier, the maximum of the heat flow peak was also the maximum cure rate. The data for EF at a variety of estimated printing temperatures was presented.

Peel Testing

Sample Preparation

The heated chamber of the printer was used to spread the silicone films within an isothermal environment. The system consists of three PID controlled space heaters with fans to circulate the air, all within an insulated box. The printing chamber and printer (Luzbot Taz 6) bed were heated

to 60°C. For all sample runs the temperature was 60 ± 1ºC (still calculating from all data) from the set temperature. Temperature data for all runs is detailed in the Appendix. A thick glass plate was set on top of the bed to provide a steadier temperature because the build plate temperature tended to unevenly distribute. To prepare the polymer samples, approximately 6.5 g of the Part A Mixture and 6.5 g of the Part B Mixture were extruded from their respective syringes at room temperature into separate sides of one mixing cup so that the two parts did not touch. Two prepared cups were pre-heated in the printing chamber for at least 20 minutes. The first pre-heated cup was placed into the Thinky ARE-310 Mixer and a timer was started. After mixing for 15 s at 2000 rpm and 15 s at 2200 rpm, the mixed silicone was quickly scooped onto the bed in front of a razor blade lifted 2 mm from the bed (lifted using 3D printed blocks). The first layer of each sample was spread across an approximately 100 mm length and 30 mm width, and a pre-cut acetate layer was placed down near the end of the spread film to prevent adhesion to the top layer. The mixing process took about 85 s, so the next pre-heated cup was placed in the mixer 85 seconds before the desired time elapsed (2.75, 4, 6, 8, 12 or 16 minutes). After mixing, the second sample was then scooped onto the same region as before but on top of the previous layer, and spread across the existing bottom layer using a razor blade raised 4 mm by 3D printed blocks. The total sample sheet was then left to cure for 12 minutes at temperature, and then removed from the glass plate. All samples were post-cured in an 80°C oven for one hour. The next day, the sample sheets were cut by hand with a steel ruler and razor blade into approximately 6.5 mm wide strips with 75 mm of adhered region past the acetate tab boundary. Sil-Poxy was then spread on both sides of the outer tab areas to help reduce slipping during testing. The acetate masks were gently removed from each sample before loading into the tensile tester.

Sample Testing

Sample test methods were based on ASTM D1876 − 08: Standard Test Method for Peel Resistance of Adhesives (T-Peel Test). Two strips of material were pulled apart from an initially T-shaped sample using a custom-built tensile testing machine (Appendix). Samples were loaded into the testing machine connected to a 10 kg (~ 98 N) load cell. The sample tabs were placed into the upper and lower grips and tightly secured. The tester then pulled the layers apart at 100 mm/min until complete separation. At least seven samples were tested per cure time. The data recorded were force, time, and extension. Force data was normalized to the average width of each sample interface. Average width was determined by taking three measurements of the interface using a microscope with a micrometer and then averaging the results (Appendix). Force per width versus extension data were plotted for each sample and an average adhesion force across the entire extension region was calculated after the initiation peak and before the break. Average adhesion force was then plotted versus time difference between printed layer deposition.

Results

Curing Kinetics

Isothermal DSC testing at 50, 60, and 70°C gave cure rate ($d\alpha/dt$) curves with average peak cure rates occurring at 3.0, 6.6, and 16.4 minutes, respectively. Total cure times for those same

temperatures were 5.8, 10.0, and 21.5 min (Figure 3a). Running integrals of the cure rate curves gave cure percent curves (Figure 3b). These curves are later used to compare cure percent with adhesive force between layers.

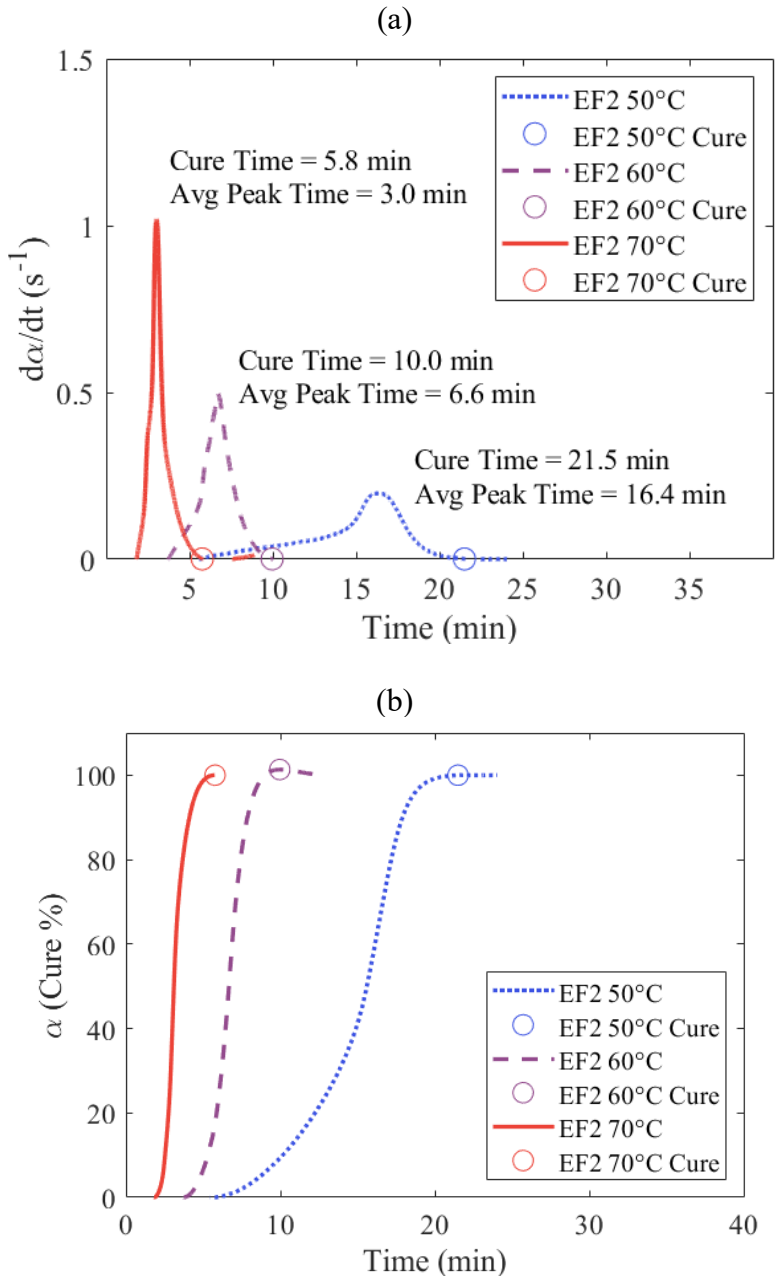

Figure 3. (a) Averaged isothermal scans of EF with cure time (noted on the graph with circles) and peak cure rate time. (b) Cure percent of EF vs. time, cure time noted on the graph with circles.

Peel Testing

Peel testing of all samples revealed a region of higher peel forces occurring at 2.75 and 4 min, (0 and 0.32% cure, respectively) and a region of lower peel forces at 6, 8, 12, and 16 min (23.6, 92.1, 100, and 100% cure, respectively). Table 1 shows the average maximum and average mean peel force values of each cure time data set. The maximum value for each sample time in the table is the mean maximum force/mm of all data in the respective set including the initiation peak. The average mean value for each sample time in the table is the mean value of all means in the respective set. Average maxima for the high force region range from 0.382 N/mm to 0.392 N/mm. Average maxima for the low force region range from 0.270 N/mm to 0.358 N/mm. Average means from the high force region range from 0.307 N/mm to 0.310 N/mm. Average means from the low force region range from 0.235 N/mm to 0.253 N/mm.

Table 1. Values of overall peel test data in terms of layer 1 cure time and layer 1 cure percent before deposition of the second layer.

Sample Time (min)	Cure Percent Before 2nd Layer (%)	Average Max (N/mm)	Average Mean (N/mm)
2.75	0	0.382	0.307
4	0.32	0.392	0.310
6	23.6	0.318	0.245
8	92.1	0.270	0.235
12	100	0.358	0.253
16	100	0.310	0.253

Figure 4a shows the force/width data for samples that did not break during peel testing. Broken sample data is shown in the Appendix to compare tensile break force to peel force. Dotted lines in Figure 4a show the initiation peak and the end data, solid lines show the data after the initial peak (the initiation of the peel) and before break. The data are artificially separated by time on the plot for clarity. The mean of each data set after the initial peak and its relationship to the experimental set is shown in Figure 4b, with the mean of all data points of the same cure time shown as a dashed line for clearer comparison. A boxplot analysis of the data in Figure 4b is shown in the Appendix. Clear groupings occur in the data means at <= 4 minutes and >= 6 minutes. These grouped means are then averaged to produce a high force region mean (0.308 N/mm) and a low force region mean (0.247 N/mm) in Figure 4c. In Figure 4c, time values are replaced with cure percent values on the x-axis. The averaged maximum and mean data for the high and low force regions are then used to calculate the expected forces at break of a range of adhesive interface widths in Figure 4d. Differences in force at break from low to high region maxima are 0.73 N at 1 cm width, 23% more than the lower maximum. Differences in force at break from low to high region means 0.62 N at 1 cm width, 25% more than the lower mean.

(a)

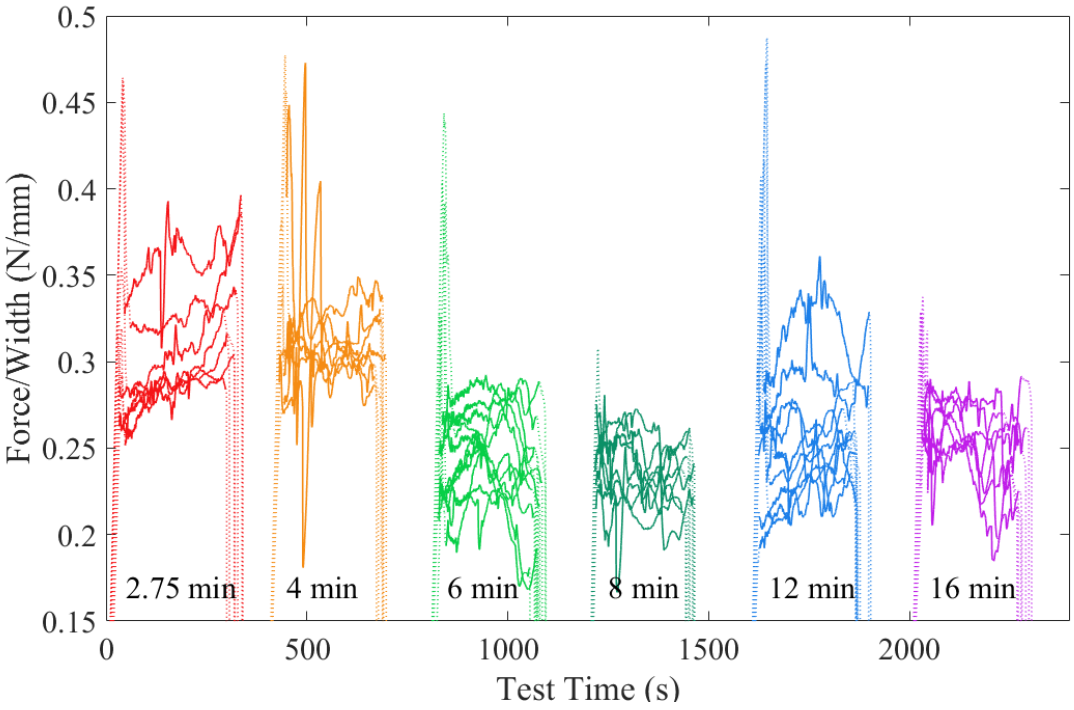
0.5
0.45
0.4
0.35
0.3
0.25
0.2
0.15
Force/Width (N/mm)
2.75 min
4 min
6 min
8 min
12 min
16 min
0
500
1000
1500
2000
Test Time (s)

(b)

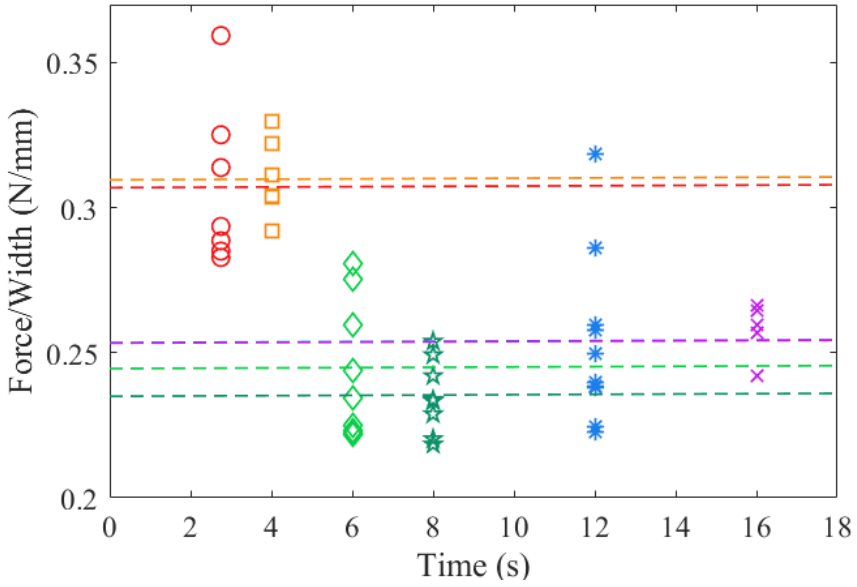
0.35
0.3
0.25
0.2
Force/Width (N/mm)
0
2
4
6
8
10
12
14
16
18
Time (s)

(c)

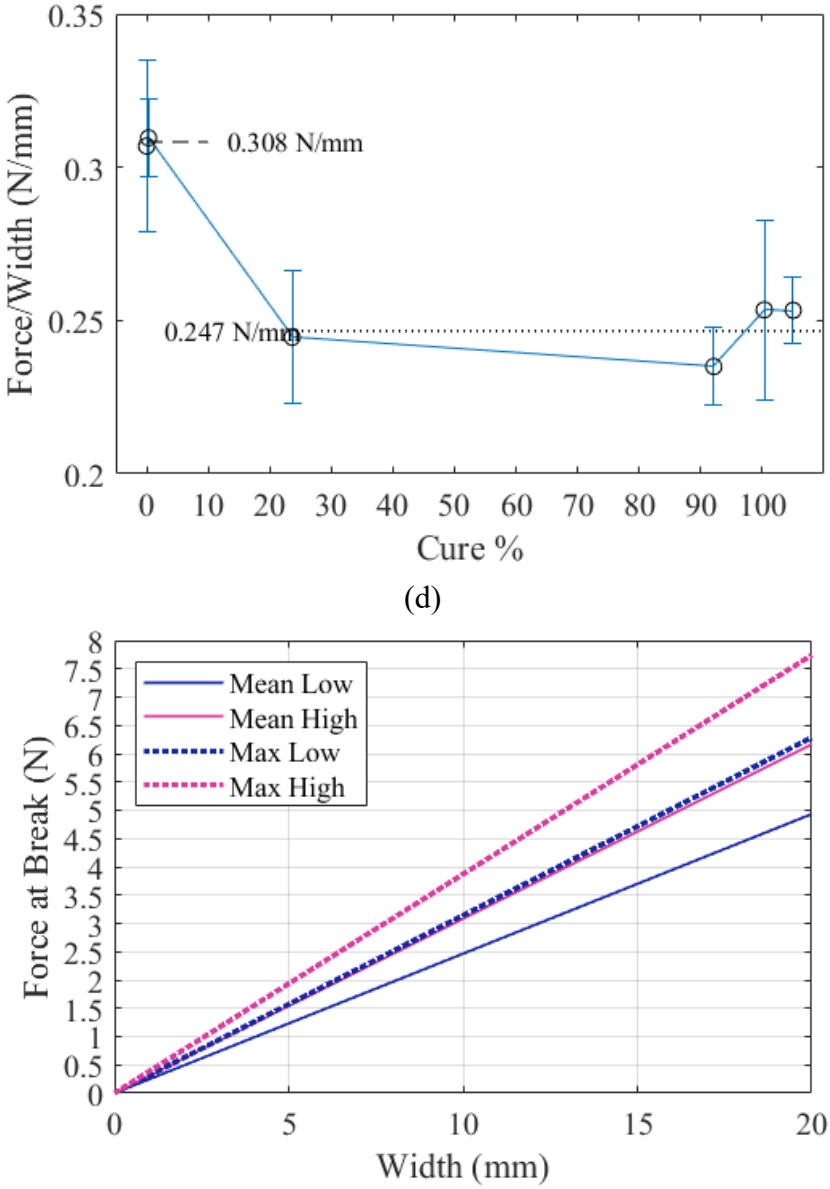

Figure 4. (a) Peel test overall data. (b) Average peel force data of each cure time. (c) Mean data of each set versus cure percent, with a connective line for trend visualization. (d) Calculated differences between mean and max forces at break for high force region (pink line) and low force region (blue line) as width of sample increases.

Discussion

Characterization of adhesion between two layers of silicone is important for both direct ink writing of thermosets as well as general fabrication methods that use silicone itself as a “glue”. For printing, predictability of final mechanical performance is integral to development of a dependable manufacturing process. Our direct ink writing method relies on layer-by-layer deposition of silicone lines. Cure percent in this in-line mixed system must be accounted for in the path planning for the printer to produce an expected range of adhesion forces layer-by-layer

across the entire part. Waiting too long before the next layer is deposited could result in unanticipated weak fracture regions because of the lower adhesive forces present at the interface. We claim that the strengths differences in the interface mainly comes from the decreasing availability of covalent bonding sites in the lower partially cured layer, decreasing the number of higher strength adhesive bonds at the interface.

The data presented here represent one specific experimental situation, but the methods and conclusions can apply to other types of thermoset materials and manufacturing systems. Adhesion between two curing materials will change based on previous layer percent cure before subsequent layer attachment. Here, the adhesive force required to separate two layers of silicone is higher when the layer is deposited before 0.32 % cure. For our silicone direct ink writing system, this four-minute boundary for higher strength parts potentially limits the cross-sectional surface area in a single printed layer to smaller regions and/or to faster printing speeds. These procedural considerations can be implemented with advanced path planning techniques to print new layers on top of acceptable cure percent regions in lower printed layers. Control of the curing process to create isotropic adhesive force throughout the printed part is a difficult proposition, especially with arbitrary, asymmetric geometries.

This work is also limited to studying the adhesion effects from 2.75 minutes (0 % cure) and onward due to the time required to mix and spread the films by hand. This 0% cure value comes from the DSC data, which at 60°C unfortunately does not reach a positive cure rate until just over three minutes. This is because the samples were not pre-heated - this was done to capture as much quantifiable curing data in the furnace as possible and reduce the amount of curing during prep outside the DSC. At room temperature (25°C), Ecoflex 00-30 takes four hours to cure[39], so two minutes (0.83% of that time) is unlikely to produce a significant cure effect during sample preparations. Keeping the samples at temperature during mixing, transfer to a syringe, measuring, loading into the pan, and clamping the pan would be unreasonable at 60°C. So, each sample required a short period of time to heat up inside the DSC furnace before heat flow values passed the cure baseline.

In peel testing, we expected cohesive failure to happen closer to 0 minutes of cure, because logically the two layers would be so close to uncured that they would behave as one bulk material. Cohesive failure did occur, especially in the lower cure region, but most samples broke before any peeling, with only two breaking further into the peel process (Appendix). Cohesive failure occurred in 46% (6 of 13) of 2.75 minute samples, 17% (2 of 12) of 4 minute samples, and 11% (2 of 19) of 6 minute samples. Even at 2.75 minutes, more than half the tested samples exhibited adhesive failure (separation along the interface) and not necessarily cohesive failure (breakage in the bulk material). Seen in the sample break data in the Appendix, the peel force (when the samples do peel) never reached the average ultimate tensile force at break of 0.59 N/mm (confirm this later). This unexpected adhesive failure occurring so low in the cure percent is worth investigating further via process alterations and higher accuracy temperature/cure experiments.

Peel test results could have been affected by several factors along with difficulty of film spreading: (1) gravitational forces causing bending in the sample end, (2) unevenness in the placement of the acetate layer boundary causing a slightly non-perpendicular start to the peel

initiation area, or (3) uneven widths of samples due to hand-cutting methods. Nevertheless, the concept of decreasing interfacial peel force with increasing cure time between layers is clearly indicated in the data, with significant differences between the higher and lower region means.

Conclusion

Building on our framework for direct ink writing of curing thermoset materials, we developed a method of characterizing the adhesive peel forces in silicone layers of varying cure percent. We showed that adhesive forces increase with decreasing cure percent between deposited layers like those in our direct ink writing system. DSC data for potential printing temperatures at 50, 60, and 70°C quantified cure rate and cure percent growth in a silicone thermoset elastomer (Ecoflex 00-30) to compare with T-Peel test data. With 60°C as the expected printing temperature, layers with less than 0.32% cure (high force region) had a 24.7% higher peel force than layers with 23.6% cure or more (low force region). At 1 cm sample width, the high force region maximum peel force is calculated to be 23% higher than the low force region maximum. For the same 1 cm width, the high force region mean is calculated to be 25% higher than the low force region mean. The unexpected occurrence of adhesive failure (peeling along the interface) versus cohesive failure even at low cure percent is worth further investigation. Quantification of adhesion versus cure percent should be incorporated into path planning for direct ink writing of curing thermoset materials to ensure predictable mechanical performance and high strength in 3D printed parts.

Checks for Steph to do:

1. Number sections after FRL review
2. Get through all the temp data + plot in Appendix
3. 10-1-19 data masses isothermal EF in Universal Analysis
4. Recheck breakage samples + determine widths

REFERENCES

1. Skylar-Scott, M. A., Mueller, J., Visser, C. W. & Lewis, J. A. Voxelated soft matter via multimaterial multinozzle 3D printing. *Nature* **575**, 330–335 (2019).
2. Yuk, H. & Zhao, X. A New 3D Printing Strategy by Harnessing Deformation, Instability, and Fracture of Viscoelastic Inks. *Adv. Mater.* **30**, n/a-n/a (2018).
3. Ober, T. J., Foresti, D. & Lewis, J. A. Active mixing of complex fluids at the microscale. *Proc. Natl. Acad. Sci.* **112**, 12293–12298 (2015).
4. Hinton, T. J., Hudson, A., Pusch, K., Lee, A. & Feinberg, A. W. 3D Printing PDMS Elastomer in a Hydrophilic Support Bath via Freeform Reversible Embedding. *ACS Biomater. Sci. Eng.* **2**, 1781–1786 (2016).
5. Bhattacharjee, T. *et al.* Writing in the granular gel medium. *Sci. Adv.* **1**, e1500655 (2015).
6. O'Bryan, C. S. *et al.* Self-assembled micro-organogels for 3D printing silicone structures. *Sci. Adv.* **3**, e1602800 (2017).
7. Frutiger, A. *et al.* Capacitive Soft Strain Sensors via Multicore–Shell Fiber Printing. *Adv. Mater.* **27**, 2440–2446 (2015).
8. Hardin, J. O., Ober, T. J., Valentine, A. D. & Lewis, J. A. Microfluidic Printheads for Multimaterial 3D Printing of Viscoelastic Inks. *Adv. Mater.* **27**, 3279–3284 (2015).

9. Roh, S., Parekh, D. P., Bharti, B., Stoyanov, S. D. & Velev, O. D. 3D Printing by Multiphase Silicone/Water Capillary Inks. *Adv. Mater.* **29**, n/a-n/a (2017).
10. Coulter, F. B. & Ianakiev, A. 4D Printing Inflatable Silicone Structures. *3D Print. Addit. Manuf.* **2**, 140–144 (2015).
11. Coulter, F. B. *et al.* Bioinspired Heart Valve Prosthesis Made by Silicone Additive Manufacturing. *Matter* **1**, 266–279 (2019).
12. Durban, M. M. *et al.* Custom 3D Printable Silicones with Tunable Stiffness. *Macromol. Rapid Commun.* n/a-n/a doi:10.1002/marc.201700563.
13. Lipton, J. I., Angle, S. & Lipson, H. 3D Printable Wax-Silicone Actuators. in *2014 Annual International Solid Freeform Fabrication Symposium* 4–6 (Laboratory for Freeform Fabrication and University of Texas Austin, TX, 2014).
14. Walker, S. *et al.* Zero-Support 3D Printing of Thermoset Silicone Via Simultaneous Control of Both Reaction Kinetics and Transient Rheology. *3D Print. Addit. Manuf.* **6**, 139–147 (2019).
15. Walker, S., Yirmibeşoğlu, O. D., Daalkhaijav, U. & Mengüç, Y. 14 - Additive manufacturing of soft robots. in *Robotic Systems and Autonomous Platforms* (eds. Walsh, S. M. & Strano, M. S.) 335–359 (Woodhead Publishing, 2019). doi:10.1016/B978-0-08-102260-3.00014-7.
16. Mazurek, P., Vudayagiri, S. & Skov, A. L. How to tailor flexible silicone elastomers with mechanical integrity: a tutorial review. *Chem. Soc. Rev.* **48**, 1448–1464 (2019).
17. Dušek, K. Diffusion control in the kinetics of cross-linking. *Polym. Gels Netw.* **4**, 383–404 (1996).
18. Simpson, T. R. E., Parbhoo, B. & Keddie, J. L. The dependence of the rate of crosslinking in poly(dimethyl siloxane) on the thickness of coatings. *Polymer* **44**, 4829–4838 (2003).
19. Polmanteer, K. E. & Lentz, C. W. Reinforcement Studies—Effect of Silica Structure on Properties and Crosslink Density. *Rubber Chem. Technol.* **48**, 795–809 (1975).
20. Cochrane, H. & Lin, C. S. The Influence of Fumed Silica Properties on the Processing, Curing, and Reinforcement Properties of Silicone Rubber. *Rubber Chem. Technol.* **66**, 48–60 (1993).
21. Cai, L.-H. *et al.* Soft Poly(dimethylsiloxane) Elastomers from Architecture-Driven Entanglement Free Design. *Adv. Mater.* **27**, 5132–5140 (2015).
22. D14 Committee. *Test Method for Peel Resistance of Adhesives (T-Peel Test)*. http://www.astm.org/cgi-bin/resolver.cgi?D1876-08R15E1 doi:10.1520/D1876-08R15E01.
23. Padhye, N., Parks, D. M., Slocum, A. H. & Trout, B. L. Enhancing the performance of the T-peel test for thin and flexible adhered laminates. *Rev. Sci. Instrum.* **87**, 085111 (2016).
24. Kinloch, A. J. & Williams, J. G. The mechanics of peel tests. in *Adhesion Science and Engineering* 273–301 (Elsevier, 2002). doi:10.1016/B978-0-444-51140-9.50035-4.
25. Rezaee, M. *et al.* Quantitative peel test for thin films/layers based on a coupled parametric and statistical study. *Sci. Rep.* **9**, 19805 (2019).
26. Chiche, A., Zhang, W., Stafford, C. M. & Karim, A. A new design for high-throughput peel tests: statistical analysis and example. *Meas. Sci. Technol.* **16**, 183–190 (2005).
27. Ebnesajjad, S. & Ebnesajjad, C. *Surface Treatment of Materials for Adhesive Bonding*. (Elsevier Science & Technology Books, 2013).
28. Morrow, J., Hemleben, S. & Menguc, Y. Directly Fabricating Soft Robotic Actuators With an Open-Source 3-D Printer. *IEEE Robot. Autom. Lett.* **2**, 277–281 (2017).

29. Yirmibesoglu, O. D. *et al.* Direct 3D Printing of Silicone Elastomer Soft Robots and Their Performance Comparison with Molded Counterparts. *2018 IEEE Int. Conf. Soft Robot. RoboSoft* (2018).
30. Schmidleithner, C. & Kalaskar, D. M. Stereolithography. in *3D Printing* (ed. Cvetković, D.) (InTech, 2018). doi:10.5772/intechopen.78147.
31. McCoul, D., Rosset, S., Schlatter, S. & Shea, H. Inkjet 3D printing of UV and thermal cure silicone elastomers for dielectric elastomer actuators. *Smart Mater. Struct.* **26**, 125022 (2017).
32. ACEO® - Unique Drop on Demand Technology with 70 Years of Silicone Knowhow. https://www.aceo3d.com/technology/.
33. Benjamin, A. D. *et al.* Light-based 3D printing of hydrogels with high-resolution channels. *Biomed. Phys. Eng. Express* **5**, 025035 (2019).
34. Smalley, D. R., Vorgitch, T. J., Manners, C. R., Hull, C. W. & VanDorin, S. L. Simultaneous multiple layer curing in stereolithography. (1997).
35. Kodama, H. Automatic method for fabricating a three-dimensional plastic model with photo-hardening polymer. *Rev. Sci. Instrum.* **52**, 1770–1773 (1981).
36. Morin, S. A. *et al.* Elastomeric Tiles for the Fabrication of Inflatable Structures. *Adv. Funct. Mater.* **24**, 5541–5549 (2014).
37. Marchese, A. D., Onal, C. D. & Rus, D. Autonomous Soft Robotic Fish Capable of Escape Maneuvers Using Fluidic Elastomer Actuators. *Soft Robot.* **1**, 75–87 (2014).
38. Shepherd, R. F. *et al.* Multigait soft robot. *Proc. Natl. Acad. Sci.* **108**, 20400–20403 (2011).
39. Ecoflex™ 00-30 Product Information. *Smooth-On, Inc.* https://www.smooth-on.com/products/ecoflex-00-30/.

Layer Adhesion Control in 3D Printed Silicone Using Curing Kinetics

Stephanie Walker[a*], Emma Lingle[a], T.J. Wallin[b], Kate Healy[b], Yiğit Mengüç[b], Joseph Davidson[a]

a. CoRIS Institute, Oregon State University, 204 Rogers Hall, Corvallis, OR 97331, USA, *walkers@oregonstate.edu (corresponding author), joseph.davidson@oregonstate.edu

b. Facebook Reality Labs, Redmond, WA, USA.

Appendix

1. Temperature control

Photos were taken of the two PID controllers every 5 seconds during each sample sheet run. MATLAB code takes each image and binarizes it. The user then picks the locations of each important region in the bitmap in MATLAB (one point to differentiate 5 or 6 in the first digit of each temperature, 7 points for digit two and three of each temperature). MATLAB code translates the bitmap values of the selected pixels (either white or black) into numbers based on pattern (Figure). Example data from one photo set is shown in Figure. Table shows all temperatures and their standard deviations. Before sample sheet run began, a FLIR thermal camera was used to determine the temperature of the top of the glass plate (Table). The average temperature and mean standard deviation for all runs was XX +/- YY °C. Still working on this.

Figure. Choosing color regions to determine temperature.

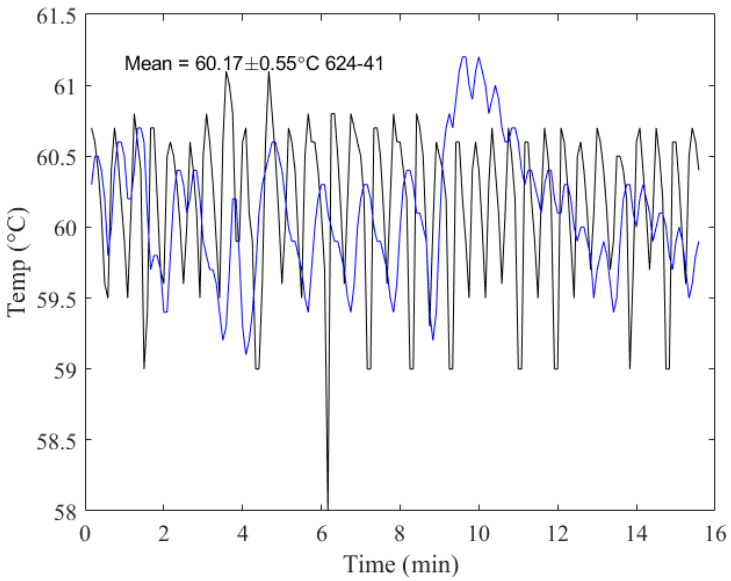

Figure. Sample temperature data from 2 PID controllers.

Table. Sample temperature data for all runs.

Sample	Mean (°C)	Stdev (°C)	FLIR (°C)
624-41	60.17	0.55	
624-42			
624-43			
624-81			
624-82			
624-83			
624-121			
624-122			
624-161			
624-162			
627-21			
627-22			
627-23			
627-61			
627-62			
627-63			

2. Equipment

The heated isothermal chamber of the existing printer was used to spread the samples within a temperature controlled environment. The samples were spread onto a glass plate using a razor blade lifted to 2 mm and then 4 mm with 3D printed blocks. The custom tensile tester was made of custom 3D printed clamps, an Open

Figure. Thermocouples were placed near the nozzle and on top of the mixer to determine temperatures at the center of the oven.

Figure. Samples were spread across a pre-heated glass plate using razor blades lifted to 2 mm and 4 mm by 3D printed blocks.

(a) (b)

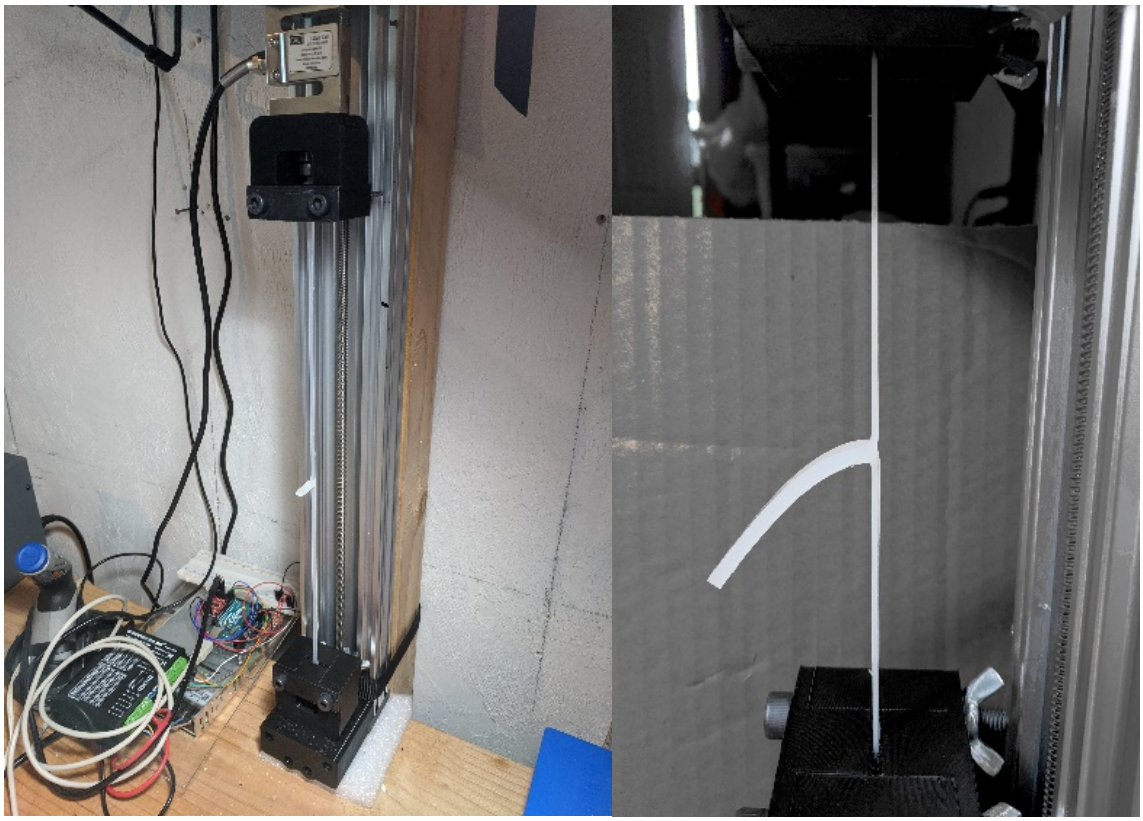

Figure. (a) A custom-built tensile tester with a 10 kg load cell was used for all peel tests. (b) T-peel test sample tabs were clamped with the rest of the sample allowed to freely move during testing.

3. Width Measurement

Interface width measurements were made with a Celestron digital microscope and a slide micrometer. First, a reference image was taken of the micrometer in focus. Then, photos of the top, middle, and bottom area of each sample interface were taken at the same magnification. The images were then rotated in Adobe Photoshop to align their edges with the x and y axes. The corrected images were then taken into Adobe Illustrator and a line was drawn across the 100 μm region of the micrometer image and each interface area image. The actual line widths were calculated using the ratio of the known value of 100 μm to the length of the drawn line in points in Adobe Illustrator. Three line lengths per sample were averaged, and the average width was used to calculate N/mm in the force data.

Figure. Measurement line thickness (red) has been exaggerated for clarity.

4. Data Analysis for Peel Testing

The following plots show the data selected for mean calculations (solid lines) versus the initiation peaks and the break points (dotted lines). Starting cut points were first minimum in the data after the initial peak. Ending cut points were the last peak in the data during break.

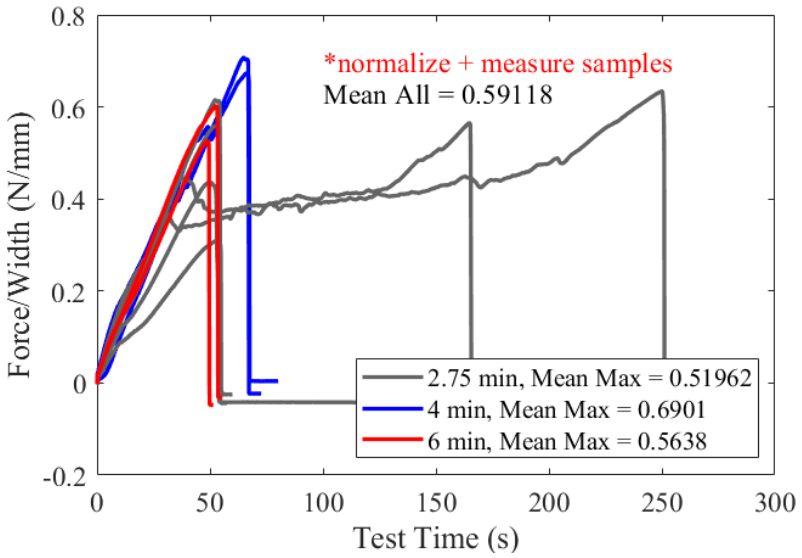

Figure. Data from samples broken during peel test. The average break force/mm was 0.59 N/mm, almost 0.2 N/mm higher than the maximum peel force seen in 2.75 and 4 minute samples.

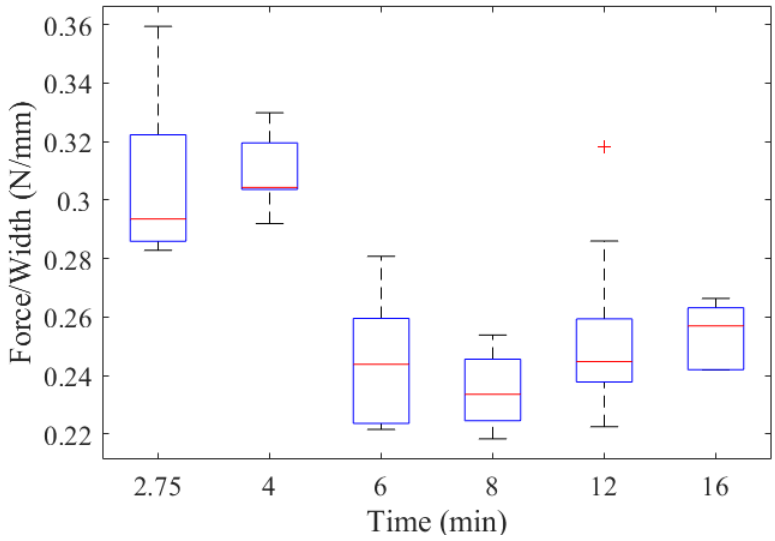

Figure. Boxplot of all peel test data, with outliers represented with a red cross.

The figures below are detailed views of all the peel test data summarized in Figure 4a in the main manuscript.

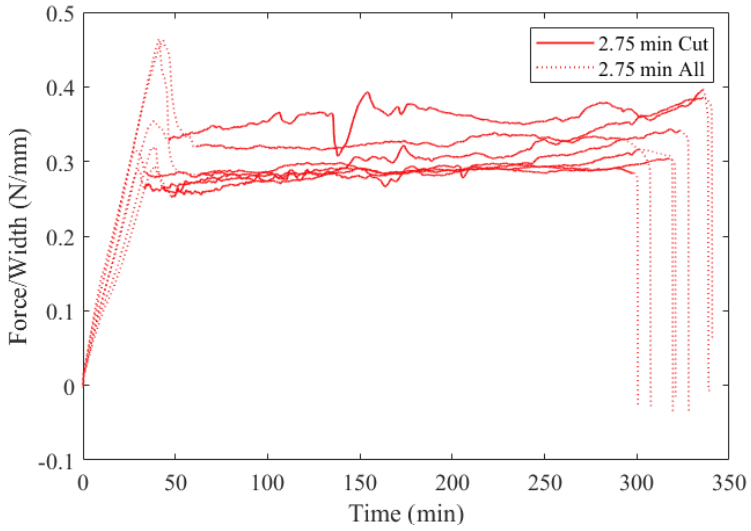
2.75 min Cut
2.75 min All
Force/Width (N/mm)
Time (min)
0.5
0.4
0.3
0.2
0.1
0
-0.1
0
50
100
150
200
250
300
350

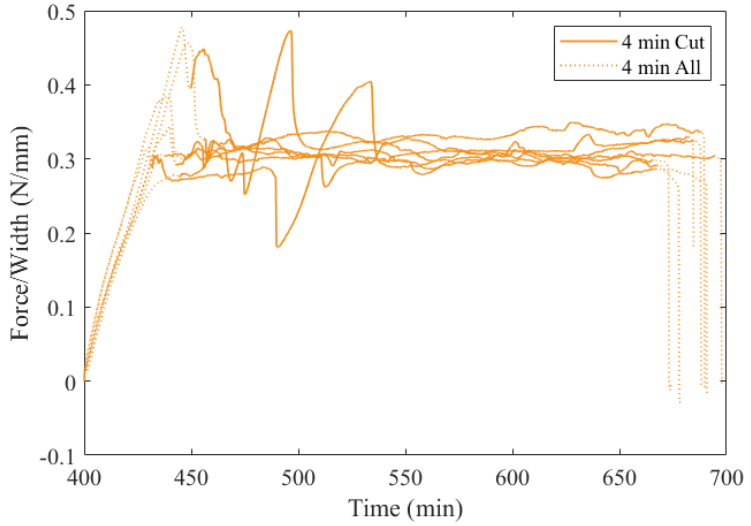
4 min Cut
4 min All
Force/Width (N/mm)
Time (min)
0.5
0.4
0.3
0.2
0.1
0
-0.1
400
450
500
550
600
650
700

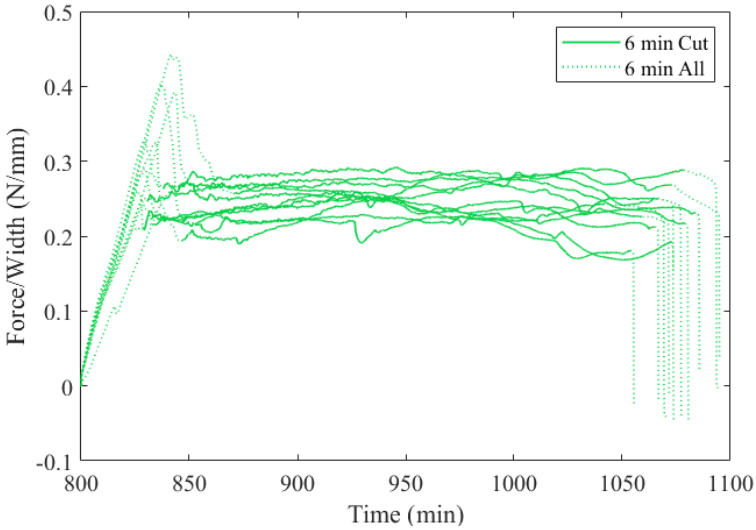
6 min Cut
6 min All
Force/Width (N/mm)
Time (min)
0.5
0.4
0.3
0.2
0.1
0
-0.1
800
850
900
950
1000
1050
1100

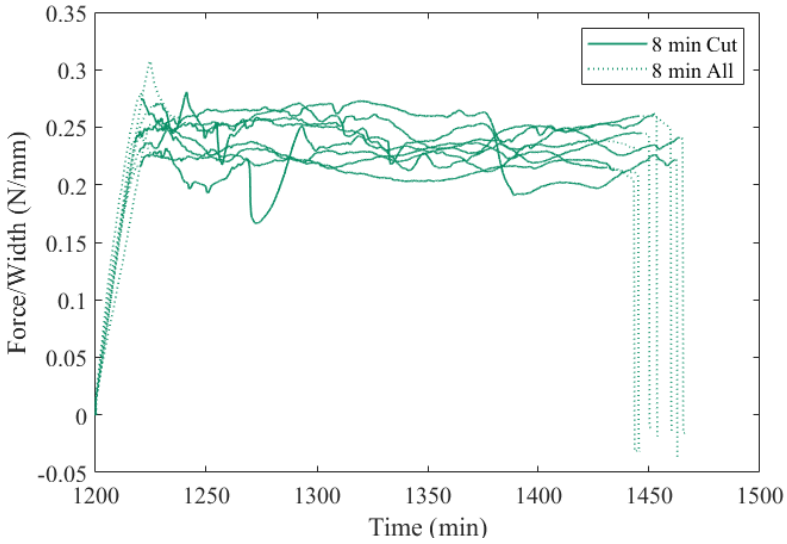
8 min Cut
8 min All
Force/Width (N/mm)
Time (min)
0.35
0.3
0.25
0.2
0.15
0.1
0.05
0
-0.05
1200
1250
1300
1350
1400
1450
1500

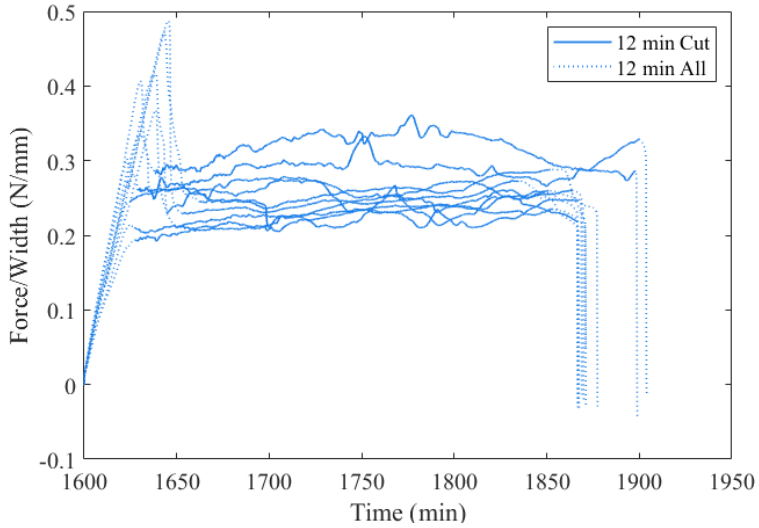
12 min Cut
12 min All
Force/Width (N/mm)
Time (min)
0.5
0.4
0.3
0.2
0.1
0
-0.1
1600
1650
1700
1750
1800
1850
1900
1950

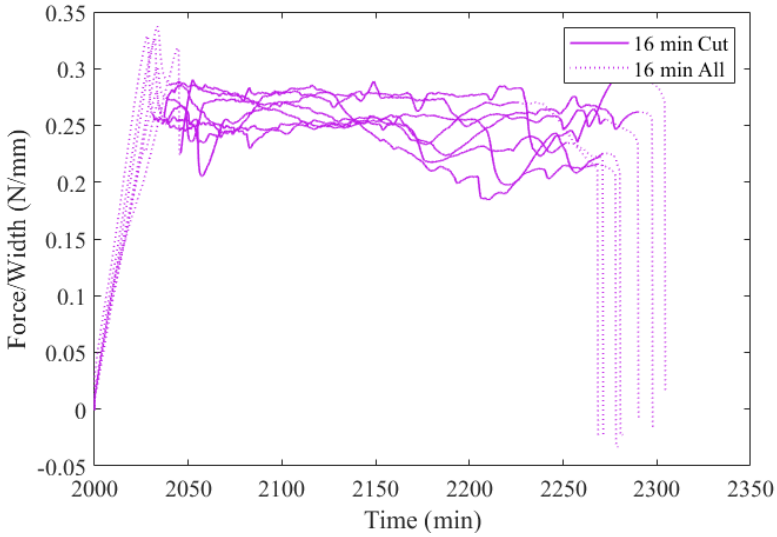
16 min Cut
16 min All
Force/Width (N/mm)
Time (min)
0.35
0.3
0.25
0.2
0.15
0.1
0.05
0
-0.05
2000
2050
2100
2150
2200
2250
2300
2350

References

1. Kenny, J. M. Determination of autocatalytic kinetic model parameters describing thermoset cure. *Journal of Applied Polymer Science* **51**, 761–764 (1994).